Sustainable Energy & Fuels

ROYAL SOCIETY OF CHEMISTRY

PAPER

View Article Online
View Journal | View Issue



Cite this: *Sustainable Energy Fuels*, 2025, **9**, 3862

# Ultra-high efficient lithium recovery *via* terephthalic acid from spent lithium-ion batteries†

Jiahui Hou, ‡[a] Zexin Wang,‡[a] Zifei Meng,[a] Jinzhao Fu,[a] Zeyi Yao, [a] Wenting Jin,[a] Xiaotu Ma, [a] Zhenzhen Yang [b] and Yan Wang *[a]

The recovery of lithium from spent lithium-ion batteries (LIBs) is a critical step in advancing sustainability within the battery industry. Traditional lithium extraction methods from end-of-life LIBs predominantly rely on chemical leaching techniques. However, these methods often involve the excessive use of acids, leading to substantial environmental concerns. Additionally, their non-selective nature can compromise the purity of the recovered lithium salt. To achieve battery-grade purity, further purification and recovery processes are necessary. In this study, we introduce a universal and eco-friendly process for lithium recovery, employing terephthalic acid to selectively extract lithium prior to the recycling of other valuable metals. This innovative method achieves lithium recovery rates exceeding 98.53% from layered oxide cathodes and 98.53% from lithium iron phosphate cathodes, delivering an exceptional purity level of 99.95%. By demonstrating applicability across a variety of cathode materials, this approach establishes a universal, sustainable and efficient solution for LIB recycling. The high-purity lithium extraction enabled by this process supports the comprehensive utilization of valuable resources, contributing significantly to the development of a circular economy for battery materials.

Received 18th April 2025
Accepted 30th May 2025

DOI: 10.1039/d5se00547g

rsc.li/sustainable-energy



## Introduction

The burgeoning production of lithium-ion batteries (LIBs) for electric vehicles (EVs) has necessitated intensive research into their efficient recycling and disposal post-use. Electric vehicles, including hybrid electric vehicles (HEV), plug-in hybrid electric vehicles (PHEV), and battery electric vehicles (BEV) rely heavily on LIBs due to their superior power, energy density, and durability. Reports indicate that the weight of a typical EV battery pack ranges from 300 to 900 kg, with LIBs having a lifespan of 8 to 10 years.[1] In 2021, there is an impressive sale of 6.75 million EVs globally, marking an increase of over 100%, with BEVs accounting for 71% of these sales.[2] This surge underscores the imminent need for the recycling of LIBs as they reach end-of-life (EOL), considering they are deemed hazardous waste but also contain recoverable valuable materials.[3]

At present, three principal pathways for recycling EOL LIBs have been identified: high-temperature treatment *via* pyrometallurgy, the leaching process through hydrometallurgy, and direct recycling that preserves the crystalline structure of the cathode materials.[4] Pre-treatment processes, essential across all recycling methods, include steps to deactivate the batteries to reduce electrical and fire hazards and separate the valuable cathode materials from other components.[5,6] The cathode active material, particularly $Li(Ni_xMn_yCo_{1-x-y})O_2$, is mainly focused due to its rich content of valuable metals like nickel, cobalt, and lithium.[7] Extensive research and numerous methodologies have been documented for the recovery of these metals from spent LIBs, reflecting comprehensive efforts to address the challenges of balancing demand and supply in the battery industry.[8]

Recently, the selective leaching of lithium (Li) from spent cathode materials has emerged as a key area of research.[9,10] Studies suggest that specific acids, which enable both leaching and precipitation, along with the use of deep eutectic solvents (DES) and oxidants, can achieve targeted Li recovery.[6,11,12] For instance, organic acid, like oxalic acid has been reported to selectively leach approximately 98% of Li from spent NCM cathodes. Concurrently, it promotes the formation of oxalate precipitates, which accumulate nickel (Ni), cobalt (Co), and manganese (Mn) in the solid residue.[13] This kind of organic acid leaching reaction can form stable complexes with lithium, which can be selectively precipitated as lithium oxalate. This compound is relatively easy to filter and purify from other metal oxalates that are less soluble. Otherwise, Inorganic acids typically dissolve the entire electrode material, requiring subsequent steps to separate lithium from other dissolved metals.[14] Additionally, formic acid and its DES variant have been employed to recover Li with an efficiency of up to 99% at 70 °C within 12 hours.[15] The use of hydrogen peroxide ($H_2O_2$) further

[a]*Department of Mechanical and Materials Engineering, Worcester Polytechnic Institute, 100 Institute Road, Worcester, MA 01609, USA. E-mail: yanwang@wpi.edu*
[b]*Chemical Sciences and Engineering Division, Argonne National Laboratory, 9700 S Cass Ave, Lemont, IL 60439, USA*

† Electronic supplementary information (ESI) available. See DOI: https://doi.org/10.1039/d5se00547g

‡ These authors contributed equally.

enhanced the redox potential of the system, allowing for the extraction of 95.4% of Li from spent lithium iron phosphate (LFP) batteries, while minimizing Fe leaching to under 1%.[16,17] Despite these advancements, most existing methods are limited to specific feedstocks, meaning they cannot be universally applied to extract lithium from all types of spent LIBs, such as NMC and LFP cathodes.[14,18] Moreover, the use of oxidants and non-recyclable acids increases both operational costs and environmental impact, posing challenges for large-scale and sustainable lithium recovery. Additionally, Table S10† summarizing lithium extraction efficiency, transition metal selectivity, and proposed mechanisms of various organic acids, including oxalic acid, citric acid, formic acid, and terephthalic acid (TPA). Among these, oxalic acid, formic acid, and TPA demonstrate selective lithium extraction from spent lithium-ion batteries. Besides, the citric acid leaching system mostly involved oxidant to fully dissolve all metals in the solution and apply solvent extraction process to separate transition metals.[19–23] However, oxalic acid also dissolves aluminium (Al), necessitating an additional purification step to produce battery-grade lithium carbonate.[24] Moreover, the formic acid leaching system is ineffective for spent LFP cathode powder, yielding a lithium leaching efficiency of less than 50%.[25] In contrast, the TPA-based method presented in this work offers a universal and highly efficient lithium extraction process applicable to a wide range of spent lithium-ion battery chemistries.

TPA (Terephthalic acid) is extensively utilized in the production of polyester, plastics manufacturing, and the fabrication of engineering resins and films.[18] In this study, we explore the introduction of TPA into a highly selective lithium extraction process that achieves minimal transition metal contamination (<1%) in the extracted solution. TPA's ability to form complexes with transition metal ions stems from its two carboxylic acid groups, which can donate electrons to these ions, thereby forming coordination compounds.[26] This specificity not only minimizes chemical waste generation but also mitigates subsequent environmental impacts. Additionally, TPA's comparatively lower toxicity than many other industrial acids simplify handling and disposal processes, thereby reducing the environmental and health risks typically associated with acid leaching processes.[27] As a primary component in the production of polyethylene terephthalate (PET), a commonly recycled plastic, the use of TPA in lithium recovery processes is aligned with sustainable practices, thereby promoting a circular economy.[28] The potential for TPA to be recovered and recycled within this process further enhances the sustainability of this method.

## Results and discussion

TPA is a promising agent for the selective extraction of lithium from spent LIBs. The selectivity is primarily attributed by ion exchange of $H^+$ in the TPA and $Li^+$ in the cathode powder, offering a novel pathway for efficient lithium separation. To optimize the conditions for TPA extraction reaction, a comprehensive study focusing on the effect of reaction pressure, reaction time and the amount of TPA excess was conducted. This investigation aimed to establish a set of parameters that maximize the extraction efficiency, thereby enhancing the overall effectiveness of lithium recovery from spent LIBs.

### Establish of the universal extraction process

For each set of extraction conditions, experiments were conducted in triplicate to determine the required reaction pressure, reaction time, and the optimal amount of TPA excess (as shown in Table S2†). The reaction pressure was calculated based on the water's saturated vapor pressure and volumetric expansion during the reaction, with a detailed calculation methodology provided in Table S3.†[29] The initial parameter optimized was the pressure; consequently, the temperature was maintained at 210 °C, which was the maximum tolerance of the PTFE jar. Additionally, the reaction duration was set to 5 hours, and the TPA was used 100% excess. As shown in Fig. S2a,† the average lithium extraction efficiency was only 26.14% at 685.33 kPa. However, as the pressure increased, a gradual improvement in extraction efficiency was observed, surpassing 99% at 2025.07 kPa. This improvement is attributed to the increased solubility of TPA under higher pressure, supported by morphological changes in TPA crystals from cubic to needle-like structures, indicating dissolution in the solvent (Fig. S1†). At higher pressures, the extraction efficiency remained stable, achieving 99.53% at 2363.6 kPa and 99.84% at 2757.13 kPa. Notably, the efficiency of transition metal extraction was consistently below 0.5%, demonstrating the process's high selectivity for lithium due to the low solubility of transition metal terephthalates.

To enhance resource utilization in the TPA extraction process, reaction time and TPA excess were optimized. As depicted in Fig. S2b,† a 4-hour reaction time maintained a high extraction efficiency of 99.84%, whereas shorter reaction times resulted in diminishing efficiencies: 96.44% at 3 hours, 86.98% at 2 hours, and 69.85% at 1 hour. Concurrently, shorter reaction times correlated with increased transition metal extraction, underscoring the need for a 4-hour reaction to maximize lithium recovery while maintaining selectivity. Similarly, the optimal TPA excess was determined. As illustrated in Fig. S2c,† the detailed calculation for the excess amount of TPA is provided in Table S4.† The amount of TPA was determined based on the molar ratio of lithium in the spent lithium-ion batteries, while the excess TPA was intended to maintain a high $H^+$ concentration in the extraction solution, thereby enhancing the reaction kinetics and overall lithium extraction efficiency.[30] The lithium extraction efficiency was 93.36% with no TPA excess. Efficiency increased with higher TPA excess and stabilized at 99.84% with a 50% excess, while transition metal extraction remained below 0.36%. Additional TPA excess did not further improve lithium extraction efficiency, establishing 50% TPA excess as optimal. Furthermore, the reaction temperature was optimized to balance extraction efficiency with reduced energy consumption. As illustrated in Fig. S2d,† a significant increase is observed between 120–140 °C. With rising temperature, the time required for the system to reach dissolution equilibrium decreases, leading to an increased concentration of $H^+$ ions in the solution, which in turn

accelerates the reaction rate.[31] Furthermore, the extraction efficiency achieved a high of 99.45 ± 0.36% within the temperature range of 180 °C to 200 °C. A decrease in reaction temperature correspondingly led to a reduction in extraction efficiency. Consequently, the optimal temperature range for the extraction process was established as 180 °C to 200 °C.

Given the diversity of materials encountered in recycling operations, the universality of the TPA extraction process was evaluated for various cathode compositions, including LMO, LCO, LFP, and black mass (a mixture of NMC111, LMO, graphite anode, and conductive carbon). As depicted in Fig. 1a–c, the SEM images reveal a reduction in particle size for LCO, LMO, and LFP compared to pristine samples. Additionally, distinct needle-shaped TPA crystals are evident in these SEM images, highlighting the morphological changes induced during the extraction process. X-ray diffraction (XRD) analysis was subsequently performed on the residue powders to further elucidate their composition. As shown in Fig. 1d, the XRD patterns clearly display prominent peaks of TPA, indicating its presence across the powders of extracted-LMO, extracted-LCO, and extracted-LFP. The residue powders were identified as $FePO_4$ in extracted-LFP, $Co_3O_4$ in extracted-LCO, and $Mn_2O_3$ in extracted-LMO, indicating a high extraction efficiency of LMO, LCO, and LFP *via* TPA. Furthermore, the extraction efficiencies are summarized in Fig. 1e. Under optimized conditions, the lithium extraction efficiencies were as follows: For LCO, 95.17% with a 0.52% extraction efficiency for Co as an impurity in the leaching solution. The efficiency for LMO reached 99.63%, with Mn impurity at only 0.47%. For LFP, the lithium extraction was slightly lower at 94.75%, accompanied by 0.10% of P and 0.13% of Fe co-dissolution. The leaching efficiency for Black Mass (BM) was 96.63%, with co-dissolution of 0.12% Ni, 0.31% Mn, and 0.17% Co in the solution. To further improve extraction efficiency for LCO, LFP, and black mass, the reaction time was extended to 6 hours. Under these adjusted conditions, the extraction efficiencies were as follows: 98.71% for LCO, 99.66% for LMO, 98.53% for LFP, and 99.81% for black mass. The impurity leaching efficiencies were 0.61% for Co from LCO, 0.48% for Mn from LMO, 0.33% for LFP (comprising 0.15% P and 0.18% Fe), and 0.65% for black mass (with 0.15% Ni, 0.33% Mn, and 0.17% Co). Overall, this study developed a universal lithium extraction method capable of selectively recovering lithium from diverse feedstocks with extraction efficiencies exceeding 98.5% while minimizing impurity leaching. This method provides a universal and sustainable solution for lithium recovery from spent LIBs.

## Mechanism of leaching process

SEM and Focused Ion Beam (FIB) cross-sectional analyses were employed to investigate the morphological characteristics of cathode materials after extraction. As depicted in Fig. 2 and S3,† the majority of secondary particles retained their spherical morphology. However, an increase in extraction pressure at a fixed extraction time resulted in a reduction in primary particle size and more pronounced surface fragmentation. Additionally, a greater presence of needle-shaped recrystallized

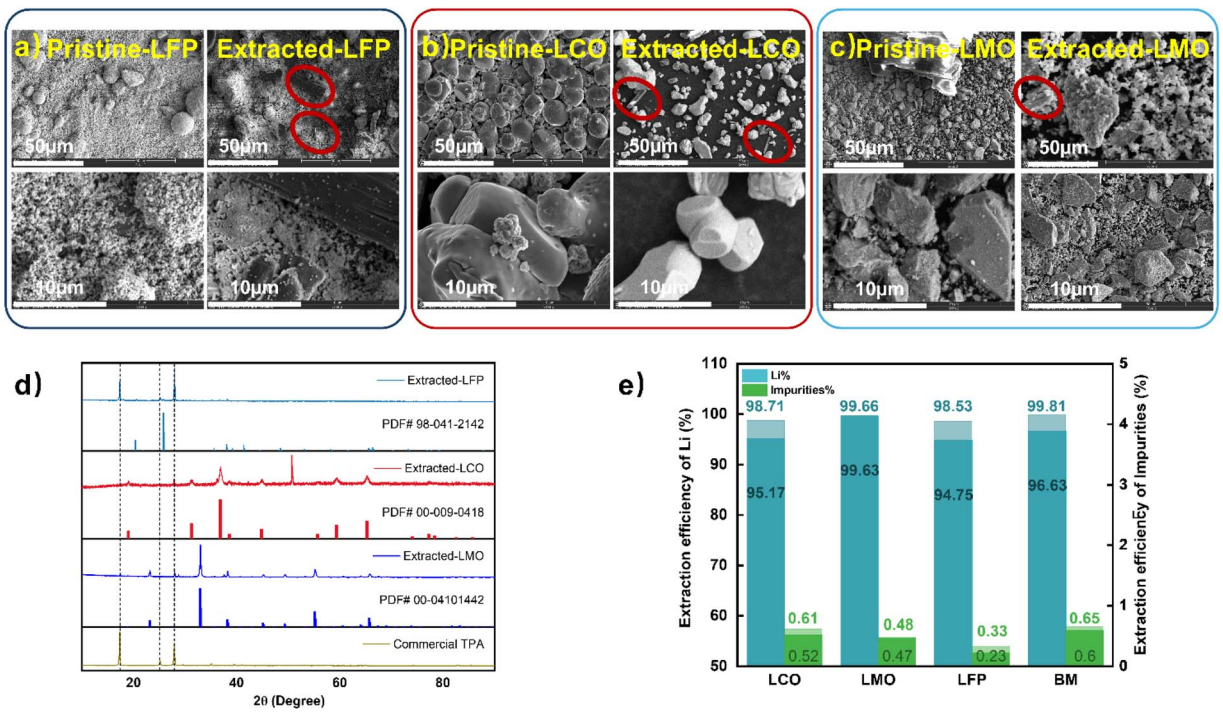


Fig. 1 (a) SEM images for pristine LFP and extracted-LFP, (b) SEM images for pristine LCO and extracted-LCO, (c) SEM images for pristine LMO and extracted-LMO, (d) XRD pattern for comparison of extracted-LFP; standard $FePO_4$, extracted-LCO; $Co_3O_4$, and extracted-LCO; $Mn_2O_3$, (e) lithium and transition metal (TM) leching efficiencies of LCO, LMO, LFP and black mass with optimized leaching conditions based on NMC cathode powder, and the leaching efficiency of LCO, LMO, LFP and black mass with adjusted parameters.

 

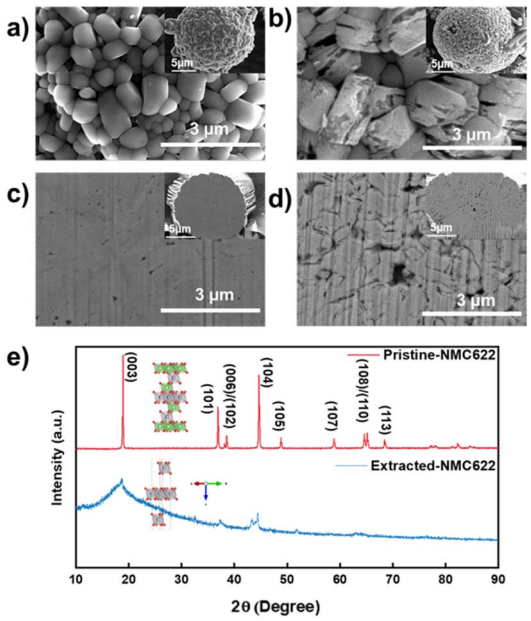


Fig. 2 (a) Morphology of primary particles for pristine NMC622, and the morphology of secondary particles for pristine NMC622 (b) morphology of primary particles for extracted NMC622 under high pressure, and the morphology of secondary particles for extracted NMC622 under high pressure, (c) the cross section for pristine NMC622 at the bulk and the whole particle, (d) the cross section for extracted NMC622 at bulk and the whole particle, (e) the XRD pattern for pristine-NMC622 and extracted-NMC622 with schematic diagram of the crystal structure.

TPA was observed with increasing pressure, indicating enhanced TPA solubility at higher pressures.[32] FIB-SEM provided detailed cross-sectional insights into the structural changes of cathode particles before and after extraction, as depicted in Fig. 2c and d. The extracted cathode material exhibited a significantly more porous structure compared to commercial NMC622, suggesting the formation of ion-extraction pathways. This observation was further supported by XRD analysis results, presented in Fig. 2e. During the delithiation process, the (003) peak becomes broader, and the (101) peak shifts toward a higher $2\theta$ position. Furthermore, the merging of the (006)/(102) and (108)/(110) peaks suggested a weakening of the layered structure.[33] Owing to the limited resolution of the XRD measurement, the (101), (006), and (102) peaks appear overlapped.[34–38] Based on the above analysis, the extracted NMC622 maintained weakened layer structure.

X-ray photoelectron spectroscopy (XPS) was employed to investigate the compositional changes in lithium (Li), carbon (C), oxygen (O), and transition metals (Ni, Mn, and Co) on the surface and in the bulk of pristine and extracted NMC622 powder. The C 1s spectra (Fig. 3a) for both pristine NMC622 and extracted NMC622, calibrated at 284.9 eV, were used as reference points for the binding energies of other elements. Peaks corresponding to C–O (286.4 eV) and C=O (290.5 eV) were associated with carbonate-like species.[39,40] The O 1s spectra (Fig. 3b) at 531.5 eV confirmed the presence of lithium carbonate on the surface of the pristine NMC622 cathode powder, while Me–O peaks at 530 eV in the bulk indicated minimal lithium carbonate presence.[25] Notably, as displayed in Fig. 3b, no $-CO_3$ peak was detected in the surface or bulk regions of the extracted NMC622, indicating effective lithium extraction. The most direct evidence of the extraction efficiency was presented by Li 1s spectrum in Fig. 3c. The two peaks located at 54.04 eV and 55.1 eV represent the residue $Li_2CO_3$ on the pristine-NMC622 surface and $Li_2O$ in the NMC622 crystal structure.[25] As mentioned in Fig. 2b and d, morphological changes are evident not only on the surface but also within the bulk of the particles, suggesting that the ion exchange between $H^+$ and $Li^+$ occurred throughout the entire secondary particles. However, in the primary particle, $Li^+$ located on the surface and subsurface regions was more readily exchanged with $H^+$, while $Li^+$ in the bulk exhibited slower reactivity.[39,41] To investigate whether ion exchange extended into the bulk of primary particle, XPS depth profile analysis was conducted. Notably, no Li-related peaks were detected either on the surface or within the etched bulk of the primary particles, indicating a complete ion exchange reaction. This conclusion is further supported by the ICP-OES results listed in Table S5,† where only 0.05 wt% of lithium was detected in the extracted NMC622, thereby confirming the complete removal of $Li^+$ *via* ion exchange.

During extraction reaction, the $Li^+$ from the pristine-NMC622 powder exchanged with $H^+$ from the TPA solution, transferring lithium into the solution. This $Li^+/H^+$ exchange protonated the oxygen lattice of the NMC622, forming a less stable H-NMC structure prone to further decomposition.[41] To maintain structural stability, partial reduction of transition metals occurred, altering their chemical states.[42] The Ni 2p spectra (Fig. 3d) presents a spin–orbit line, with Ni $2p_{3/2}$ located at 854 eV confirming the presence of $Ni^{2+}$. The peak at 855.8 eV ($2p_{3/2}$) corresponding to $Ni^{3+}$ in pristine-NMC622 powder.[43] After the extraction reaction, only the $Ni^{2+}$ peak was detected on the surface of the extracted NMC622 powder. Meanwhile, in the bulk of the extracted NMC622 powder, the ratio of $Ni^{2+}$ increased to 66.71%, higher than in the pristine NMC622 powder (48.05%). Therefore, the average chemical state of Ni decreased from +2.52 to +2.33. For Mn, the 2p binding energy peaks (Fig. S4a†) at 641 eV indicated $Mn^{3+}$, while peaks at 643 eV confirmed $Mn^{4+}$ in both pristine and extracted NMC622.[44] The average Mn oxidation state decreased slightly, from +3.82 to +3.81, and no $Mn^{2+}$ was detected in the surface or bulk regions of the extracted NMC622, indicating no formation of transition metal terephthalates during the extraction process. The Co 2p XPS spectra (Fig. S4b†) demonstrated changes in the Co cation's valence states. The Co 2p3/2 peaks at 779.8 eV and 781.5 eV corresponded to $Co^{3+}$ and $Co^{2+}$, respectively.[44] After extraction, the proportion of $Co^{3+}$ decreased, resulting in a reduction of the average Co oxidation state from +2.78 to +2.67.

Energy Dispersive X-ray Spectroscopy (EDS) mapping, presented in Fig. S5 and S6,† was utilized to investigate the elemental distribution within the cross-sections of pristine NMC622 and extracted NMC622. The analysis revealed that the transition metal distribution in the extracted NMC622 closely aligned with that of the pristine material, indicating that most transition metals did not react with TPA to form transition

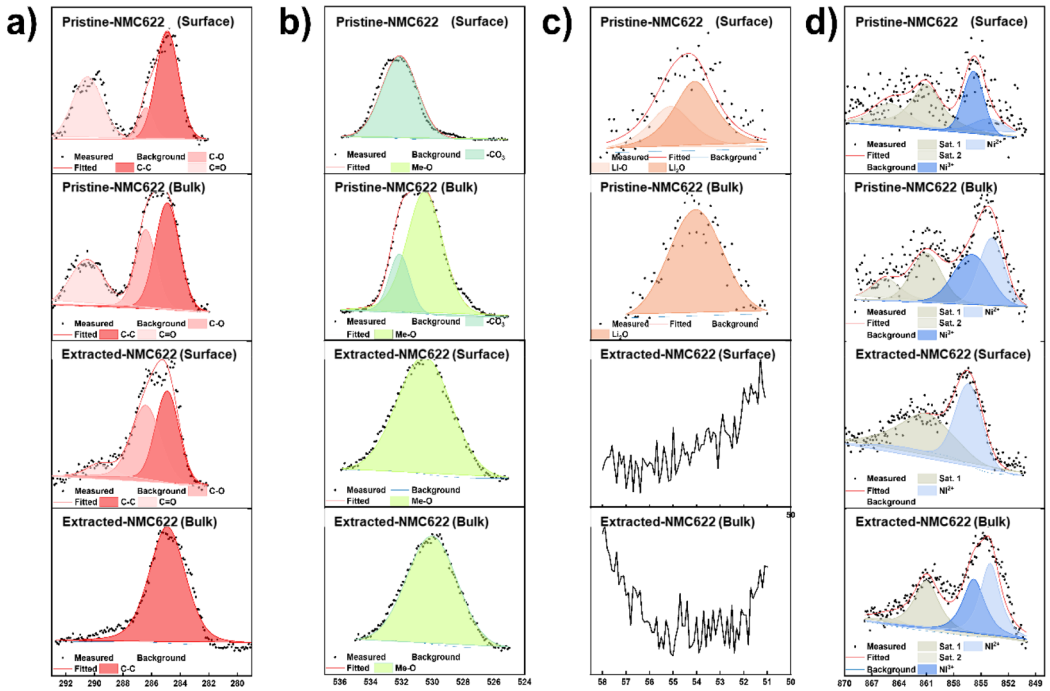


Fig. 3 XPS spectra for (a) C 1s of pristine-NMC622 and extracted-NMC622 on the surface and in the bulk, (b) O 1s of pristine-NMC622 and extracted-NMC622 on the surface and in the bulk, (c) Li 1s of pristine-NMC622 and extracted-NMC622 on the surface and in the bulk, and (d) Ni 2p of pristine-NMC622 and extracted-NMC622 on the surface and in the bulk.

metal terephthalates. Moreover, transition metal terephthalates can form through coordination between the carboxyl groups of TPA and transition metal ions, resulting in metal–organic coordination complexes.[45] However, in this lithium extraction process, the formation of transition metal terephthalates was limited due to the low concentration of transition metal ions present. Additionally, signals attributed to Al were identified as the coatings or doping materials used in commercial NMC622, while the detection of Ga and Pt signals was attributed to the polishing source and protective layers applied during sample preparation.

As depicted in Fig. 4, the extraction reaction involved an ion exchange between $Li^+$ ions from the NMC622 crystal structure and $H^+$ ions from the TPA solution. This exchange led to a decrease in the average chemical state of the transition metals, which dropped from +3.04 to +2.94. The extraction reaction mechanism is summarized in eqn (3).

$$LiTMO_2 + H^+ \rightarrow Li^+ + TMO_{1.47} + 0.5H_2O + 0.265\ O_2 \quad (3)$$

## Lithium recovery

Following the extraction of lithium into the solution, accompanied by the trace amounts of transition metal terephthalates, those organic compounds were identified *via* $^{13}C$ NMR spectroscopy. As depicted in Fig. 5a, characteristic signals at 128.6 ppm (attributed to CH in the phenylene group), 138.56 ppm (corresponding to the phenyl C adjacent to COOLi), and 175.16 ppm (associated with COOLi) were observed.[46] These spectroscopic results confirmed the formation of $Li_2TP$ in the extraction reaction. The $Li_2TP$ solution was further recrystallized to obtain $Li_2TP$ powder by introducing acetone into the extraction solution, precipitating $Li_2TP$ due to its low solubility in acetone. The precipitated $Li_2TP$ was subsequently filtered and dried in a conventional oven. SEM analysis of the recrystallized $Li_2TP$ revealed a distinct solid block-shaped morphology, as shown in Fig. 5b. Complementary EDS

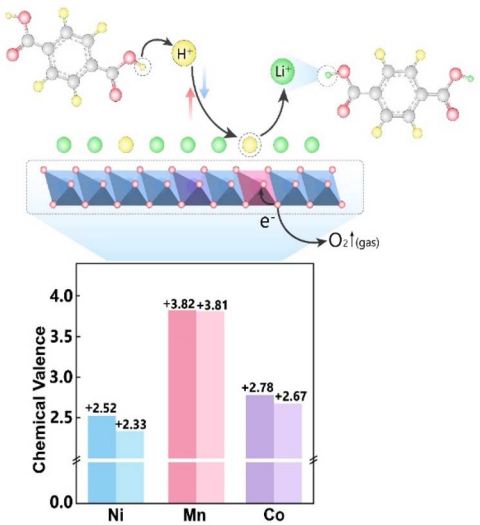


Fig. 4 Schematic diagram for the mechanism of lithium recovery process for ion exchange reaction and the changes of the chemical state of the transition metals.

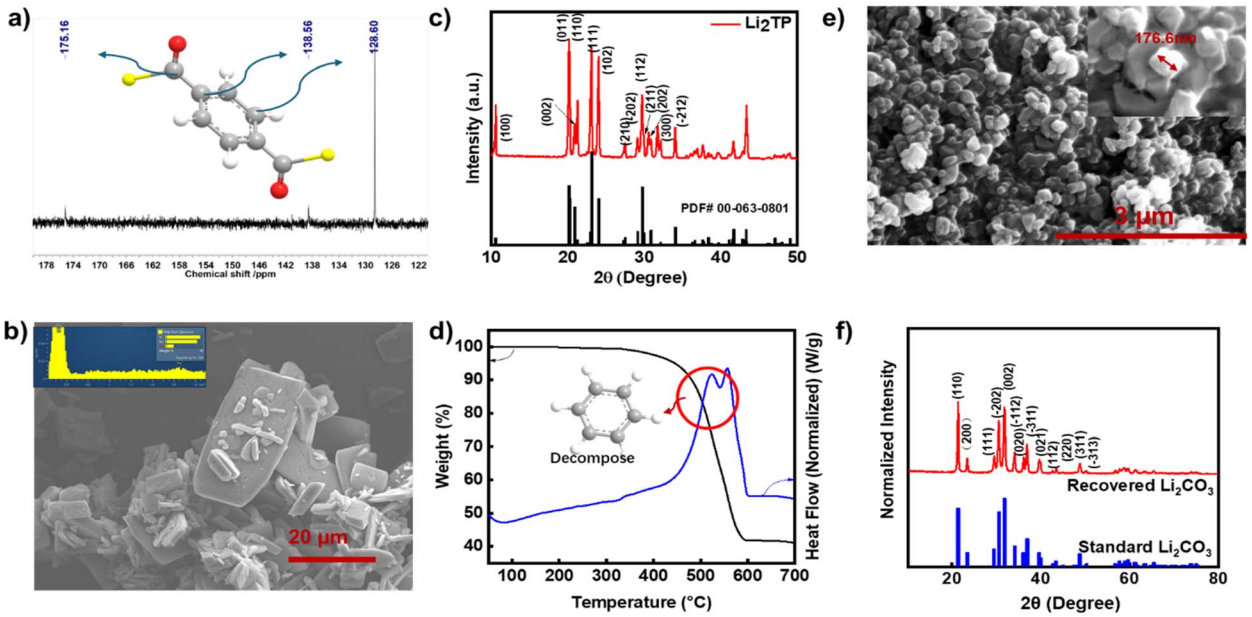


Fig. 5 (a) $^{13}$C NMR for extracted solution, (b) the morphology of recrystallized $Li_2TP$, (c) the structure of recrystallized $Li_2TP$, (d) TGA for recrystallized $Li_2TP$, (e) the morphology of recovered $Li_2CO_3$ (f) the structure of recovered $Li_2CO_3$.

mapping (Fig. S7†) identified the presence of oxygen and carbon, with no detectable transition metal peaks, indicating minimal transition metal extraction in the recrystallized $Li_2TP$. Furthermore, the ICP-OES was conducted to quantitatively determine the purity of the $Li_2TP$ powder, as shown in Table S6,† the purity of $Li_2TP$ was determined by eqn (4):

$$\text{purity of } Li_2TP = \frac{\frac{1}{2} \times C_{Li} \times M_{Li_2TP}}{m_{Li_2TP}} \quad (4)$$

Here, $C_{Li}$ represents the concentration of lithium obtained from the ICP-OES test, $M_{Li_2TP}$ represents the molar mass of dilithium terephthalate, and $m_{Li_2TP}$ represents the weight of the dilithium terephthalate powder dissolved for the ICP-OES testing. Based on the above calculation, the purity of the Li2TP powder was 96.13%.

XRD analysis confirmed the crystalline structure of the recrystallized $Li_2TP$, with its pattern aligning well with the standard $Li_2TP$ pattern (PDF# 00-063-0801) (Fig. 5c),[47] supporting the conclusion that the recrystallized $Li_2TP$ contained only trace levels of transition metals.

The $Li_2TP$ powder was subsequently converted to $Li_2CO_3$ through sintering and recrystallization. Sintering decomposed $Li_2TP$ into lithium carbonate, manganese oxide, cobalt oxide, and nickel oxide. Thermogravimetric Analysis (TGA) (Fig. 5d) confirmed the decomposition temperature of the terephthalate salt mixture, with weight loss beginning above 300 °C, indicating the absence of crystal water in the recrystallized Li2TP. Notably, two exothermic peaks observed at 524 °C and 558 °C were attributed to the disruption of benzene rings during the thermal decomposition process.[48] The observed weight loss of approximately 59% closely matched the theoretical weight loss expected during the conversion of $Li_2TP$ to $Li_2CO_3$. Post-sintering, the resultant powder was immersed in water to dissolve $Li_2CO_3$, leaving transition metal oxides as insoluble precipitates. Filtration effectively separated the metal oxides from the $Li_2CO_3$ solution. The lithium carbonate rich solution was then mixed with acetone, causing the precipitation of pure lithium carbonate due to its insolubility in acetone. After filtration, pure lithium carbonate was obtained. SEM analysis compared the morphology of commercial and recovered lithium carbonate, revealing that the latter exhibited smaller, more uniform particle sizes, potentially improving dispersion in precursor mixtures (Fig. 5e and S8†). The XRD pattern of the recovered lithium carbonate matched the standard lithium carbonate pattern (00-022-1141), as shown in Fig. 5f. To assess purity, XRF and ICP-OES analyses were conducted, using commercial lithium carbonate as a reference. As detailed in Table S6,† XRF results indicated slightly higher concentrations of impurities such as S, Ca, Ti, Mn, Fe, Ni, Cu, and Zn in the recovered lithium carbonate compared to the commercial sample, likely due to its smaller particle size.[49] However, ICP-OES analysis, performed on equal amounts of recovered and commercial lithium carbonate dissolved in aqua regia, revealed significantly lower impurity levels in the recovered lithium carbonate, indicating higher purity. The purity of the recovered lithium carbonate was determined to be 99.90%, surpassing the purity of the commercial lithium carbonate, which was 99.84%.

## Electrochemical performance of NMC622 with all recycled materials

To evaluate the recovered lithium carbonate, a batch of $LiNi_{0.6}Mn_{0.2}Co_{0.2}O_2$ (R-NMC622) was synthesized using the recovered lithium carbonate and a recycled NMC622 precursor. For comparison, a control sample, V-NMC622, was prepared using commercial lithium carbonate and the same recycled precursor. The sintering process was conducted at 450 °C for 5

hours, followed by an increase to 850 °C for 18 hours. Subsequently, the cathode powders were vacuum dried at 120 °C for 12 hours. These preparations facilitated the fabrication of cells to evaluate their electrochemical performance. SEM images of R-NMC622 and V-NMC622 (Fig. 6a) revealed typical spherical secondary particles composed of primary particles. XRD analysis and refinement (Fig. 6b and S9†) confirmed that both R-NMC622 and V-NMC622 exhibited diffraction peaks characteristic of the $\alpha$-$NaFeO_2$ structure within the *R3m* space group. Structural parameters derived from XRD refinement, listed in Table S7,† indicated comparable lattice parameters, cell volumes, and nickel migration levels for both samples, with identical cation mixing levels of 3.66%.

The electrochemical performance of R-NMC622 and V-NMC622 was evaluated in single-layer pouch (SLP) full cells under standard industrial conditions, with an electrode loading exceeding 18 mg $cm^{-2}$. Initial charge/discharge tests (2.8–4.2 V, Fig. 6c) showed that R-NMC622 achieved an initial discharge specific capacity of 173.3 mA h $g^{-1}$ and a coulombic efficiency of 86.91%, comparable to V-NMC622 at 173.5 mA h $g^{-1}$ and 85.05%, respectively. For high-rate performance (Fig. 6d), R-NMC622 exhibited similar discharge capacities to commercial NMC622 at various rates: 168.9 *vs.* 167.6 mA h $g^{-1}$ (0.1C), 162.6 *vs.* 161.6 mA h $g^{-1}$ (0.2C), 157.3 *vs.* 156.6 mA h $g^{-1}$ (0.33C), 153.2 *vs.* 152.3 mA h $g^{-1}$ (0.5C), 129.4 *vs.* 126.5 mA h $g^{-1}$ (1C), and 68.9 *vs.* 69.1 mA h $g^{-1}$ (2C). These results highlight the comparable performance of recycled materials to commercial alternatives. Cycling performance (Fig. 6e and f) was tested at 0.5C. Both R-NMC622 and V-NMC622 exhibited stable cycling behaviour, with capacity retention of 93.27% and 92.79%, respectively, after 200 cycles. Ambient temperature fluctuations caused slight capacity increases around 200 and 450 cycles. After 500 cycles, capacity retention reached 95.37% for R-NMC622 and 95.32% for V-NMC622, though V-NMC622 temporarily peaked at 95.59% due to elevated temperatures.

## Carbon footprint analysis and cost analysis

To evaluate the economic and environmental benefits of the lithium recovery process studied, both carbon footprint and cost analyses were conducted. The primary focus was on the use of chemicals, given their contribution to embodied energy and carbon footprint.[50] To develop a sustainable closed-loop recycling process, recycling and reusing TPA residue were prioritized. In practical applications, the feedstock for the TPA-lithium recovery process consisted of black mass, which included cathode materials, anode materials, and current collectors. After lithium recovery, the residual TPA was mixed with the solid-phase residue containing transition metal oxides, anode materials, and current collectors. Recycling TPA leveraged the solubility differences among these compounds. Dimethyl sulfoxide (DMSO) was selected as the solvent for its high solubility for TPA (20 g per 100 ml).[51] After filtration, the DMSO solution containing dissolved TPA was separated from the anode materials and current collectors. TPA was subsequently recovered through recrystallization with water. Fig. S10† shows that the recovered TPA had smaller particle sizes compared to pristine TPA. EDS mapping revealed no

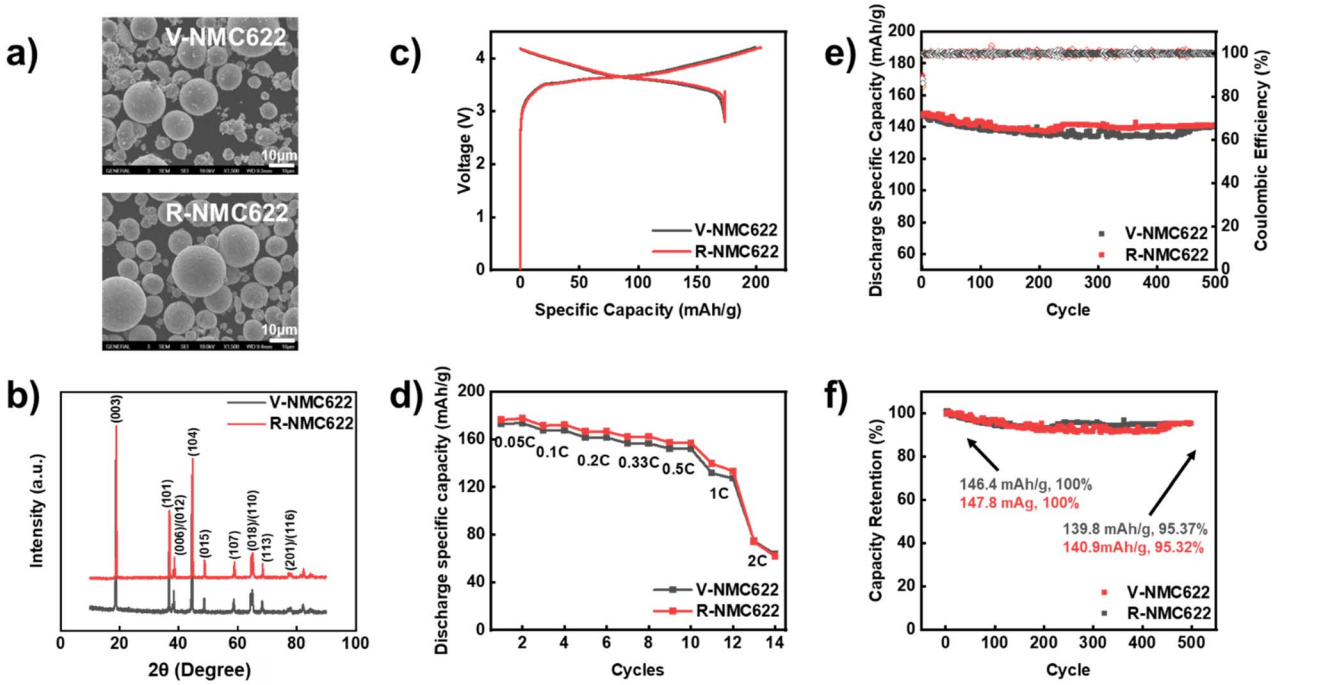


Fig. 6 (a) SEM images for V-NMC622 cathode powder and R-NMC622 cathode powder, (b) XRD pattern comparison for R-NMC622 powder and V-NMC622 powder, (c) formation comparison for R-NMC622 powder and V-NMC622 powder, (d) rate performance comparison for R-NMC622 powder and V-NMC622 powder, (e) cyclic performance comparison for R-NMC622 powder and V-NMC622 powder, and (f) discharge specific capacity retention comparison for V-NMC622 and R-NMC622 powder.

 

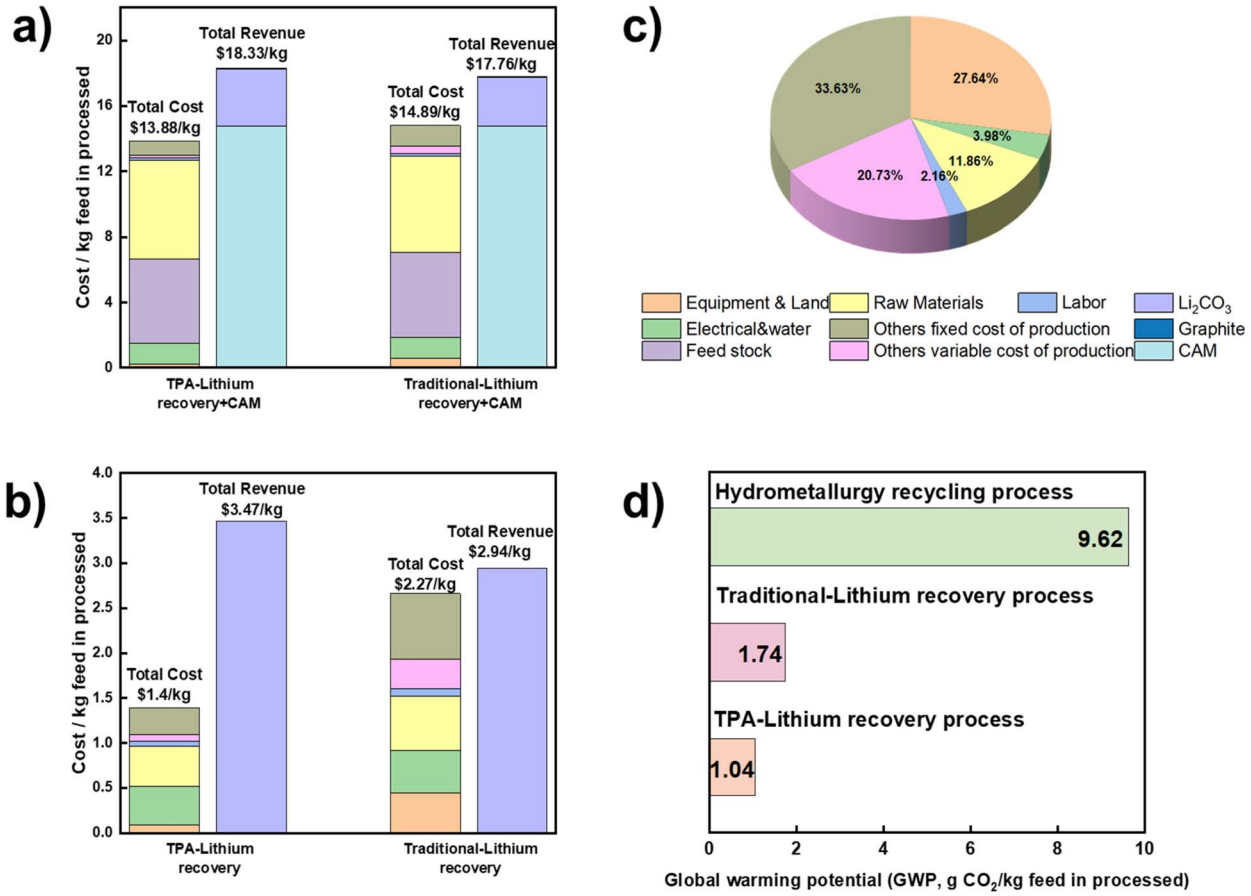


Fig. 7 Cost analysis for different recycle and recover processes. (a) total cost and total revenue comparison for TPA-lithium recovery process with CAM synthesizing process and traditional-lithium recovery process with CAK synthesizing process; (b) total cost and total revenue comparison for TPA-lithium recovery process and traditional-lithium recovery process; (c) cost difference of TPA-lithium recovery process and traditional-lithium recovery process; (d) global warming potential comparison for cathode synthesizing process, traditional-lithium recovery process, and TPA-lithium recovery process.

detectable metal impurities, suggesting high purity. ICP-OES analysis (Table S8†) confirmed that the purity of the first recovered TPA (1st R-TPA) slightly decreased from 99.82% to 98.79%, due to minor sulfur, manganese, cobalt, and nickel impurities introduced by DMSO and cathode materials. However, the purity remained stable over ten reuse cycles. To test the performance of recovered TPA with higher impurity levels, lithium extraction was performed under the same conditions as pristine TPA. Fig. S11† demonstrates that the lithium extraction efficiency of the 10th cycle of recovered TPA is comparable to that of raw TPA, achieving 99.81% *versus* 99.62%, albeit with a slightly higher impurity level in the solution (1.50% *versus* 0.23%). Furthermore, the 20th cycle of recovered TPA maintained a robust lithium extraction efficiency of 99.53% and a transition metal extraction efficiency of 1.73%. Moreover, the XRD and NMR results confirmed the retention of crystallinity and functional groups. These results highlight the stability and long-term reusability of recycled TPA as an extraction agent, underlining its economic advantages in the lithium recovery process.

The cost analysis was conducted using the EverBatt model from Argonne National Laboratory, incorporating data from the best available sources, and compared to the traditional hydrometallurgical process. This cost model accounted for the entire recycling process, including lithium recovery, precursor synthesis, and cathode synthesis stages. The TPA-lithium recovery process, described in Fig. S12 and S13,† was compared to the traditional lithium recovery process (Fig. S14 and S15†), which uses sodium carbonate precipitation and carbon dioxide purification to produce battery-grade lithium carbonate.[52] The precursor and cathode synthesis methods were identical for both processes, as detailed in previous research.[53] Key results are summarized in Tables S9 and S10† and illustrated in Fig. 7a. For a 30 000-ton per year NMC622 black mass feedstock, the TPA process achieved lower costs ($13.88 per kg feed processed) compared to the traditional process ($14.89 per kg feed processed) and higher revenues ($18.33 per kg feed processed *vs.* $17.76 per kg feed processed). While lithium is not the most valuable component of spent lithium-ion batteries, the TPA-lithium recovery process increased total revenue by 3.2%. A detailed cost breakdown (Fig. 7b) revealed that the traditional process had higher costs ($2.27 per kg feed processed), 38.33% greater than the TPA process. The TPA process also demonstrated a total revenue advantage of 18.03%.

Cost differences, highlighted in Fig. 7c, stemmed from raw materials, equipment, and land usage. The traditional process required additional chemicals such as sodium hydroxide (NaOH), sodium carbonate ($Na_2CO_3$), and $CO_2$, which, despite their lower unit costs (*e.g.*, NaOH: \$0.45 per kg, $Na_2CO_3$: \$0.14 per kg, $CO_2$: \$0.27 per kg), led to higher overall raw material expenses (\$0.599 per kg) compared to the TPA process (\$0.448 per kg).[54] This is due to the recyclability and reusability of TPA, which significantly reduce raw material costs. Additionally, the equipment costs for the TPA-based process (\$0.228 per kg of feedstock processed) were significantly lower, by 60.6%, than those for the traditional lithium recovery process (\$0.579 per kg of feedstock processed). Furthermore, although the TPA-based process requires higher operating temperatures, its shorter reaction duration and lower-temperature recovery steps contribute to reduced overall energy consumption, leading to a 21.05% decrease in electricity usage. In addition, the simplified lithium recovery process eliminates the need for lithium carbonate precipitation, significantly reducing water consumption. As a result, the costs associated with water usage and wastewater treatment were reduced by 18.75%. The expenses for electricity and water in the TPA-based process were \$0.427 per kg of feedstock processed, which is 10.45% less than those in the traditional process (\$0.477 per kg of feedstock processed). Additionally, the traditional process required high-temperature concentration, separation, and purification steps, leading to higher equipment, labor, and electricity costs, as well as increased wastewater production.

These inefficiencies also translated into higher greenhouse gas (GHG) emissions. Fig. 7d shows that precursor and cathode synthesis were the primary contributors to GHG emissions, due to long heating processes during co-precipitation and high-temperature sintering. Although GHG emissions from lithium recovery itself accounted for only 15.32% (traditional) and 9.75% (TPA) of the total recycling process, the TPA process significantly reduced emissions. Unlike the traditional method, the TPA-lithium recovery process did not require feed solution concentration or long-term heating for lithium bicarbonate decomposition. This reduced GHG emissions from 1.74 g $CO_2$ per kg feed processed (traditional) to 1.04 g $CO_2$ per kg feed processed (TPA).

# Conclusion

This study presents a highly selective terephthalic acid-based process for lithium recovery from spent lithium-ion batteries (LIBs). The method achieves outstanding efficiency, recovering approximately 99% of lithium from various layered cathode materials under 2057 kPa over 5 hours, using a 40% excess of terephthalic acid (TPA). Additionally, over 98% lithium extraction efficiency is achieved for lithium iron phosphate (LFP) materials under the same conditions, with minimal co-extraction of other elements (<1%), highlighting the method's broad applicability across different cathode types. Through subsequent recrystallization and sintering, the resulting lithium carbonate attains a purity of 99.95% with an impressive overall recycling efficiency of 98%. The process further ensures sustainability by enabling the recovery and reuse of TPA, eliminating liquid waste production. Economically, the TPA-lithium recovery process reduces costs by 38.33% compared to traditional methods while cutting greenhouse gas (GHG) emissions by 38.51%. In conclusion, this universal, innovative and sustainable methodology offers a closed-loop, environmentally friendly, and cost-effective approach to lithium recovery. By achieving 98.5% recovery efficiency with 99.95% purity, it provides a transformative solution for advancing the circular economy of battery materials and addressing critical challenges in LIB recycling.

Future research should explore the recrystallization and purification steps to reduce transition metal contamination and enhance the structural integrity of regenerated TPA. Moreover, for large-scale industrial applications, it is crucial to further optimize the parameters of the extraction reaction to maximize efficiency and minimize costs. Economic analyses based on real-scale operations in a factory setting could evaluate the feasibility and operational costs of this process. Additionally, this lithium recovery technique could be integrated with an upcycling process to build a porous structure in the transition metal oxide, enhancing diffusion paths for transition metals during the sintering process.

# Experimental

### Materials

Terephthalic acid (TPA), acetone, commercial lithium carbonate ($Li_2CO_3$), dimethyl sulfoxide (DMSO), $LiNi_{1/3}Mn_{1/3}Co_{1/3}O_2$ (NMC111, MTI), $LiNi_{0.6}Mn_{0.2}Co_{0.2}O_2$ (NMC622, Umicore), $LiNi_{0.8}Mn_{0.1}Co_{0.1}O_2$ (NMC811, MTI), $LiCoO_2$ (LCO, MTI), $LiMn_2O_4$(LMO, MTI), $LiFePO_4$ (LFP, MTI), and black mass (actual spent LIB powder including mixed cathode materials, graphite, conductive carbon, commercial recycler) were used in the extraction process. All materials used in the extraction process were dissolved in the Aqua Regia to determine the stoichiometric ratio of the elements by inductively coupled plasma-optical emission spectrometry (ICP-OES). The results were listed in Table S1.† Dimethyl sulfoxide (Sigma, >99.7%) was used to recycle residue TPA in the leachate, and the acetone (Sigma, 99.5) was used to recrystallize lithium carbonate. Lithium carbonate (Sigma, battery grade, >99.9%) was used to compare with recovered lithium carbonate.

### Recycling and recovering process

The comprehensive process of recycling and recovery was executed within a hydrothermal reactor to maintain designed pressure. The TPA powder and cathode materials were first thoroughly mixed using a mortar for 10 minutes to ensure homogeneous distribution of TPA among the cathode particles. The resulting mixture was then transferred to a PTFE jar. After adding the predetermined amount of water, the jar was sealed within a stainless-steel autoclave reactor and subsequently heated to the desired temperatures. The solubility of terephthalic acid (TPA) under ambient condition is notably low across various organic and inorganic solvents.[51,55,56] However, the

 

solubility can be significantly increased at high pressure.[57] Experimental parameters, including pressure, reaction time, and excess of TPA were varied to ascertain the optimal condition for extraction.

Following the extraction reaction, dilithium terephthalate ($Li_2TP$), along with trace amounts of transition metal terephthalates, was dissolved in the solvent and subsequently separated *via* filtration.[58] The obtained solution was transferred into acetone solution to facilitate the recrystallization of crude $Li_2TP$ powder. The residual substance, comprising unreacted TPA and transition metal oxides, was processed in dimethyl sulfoxide (DMSO) solution to recycle unreacted TPA.[51] After filtration and recrystallization in water, TPA was effectively recovered and separated from transition metal oxide residues. $Li_2TP$ powder was sintered to recover $Li_2CO_3$ in air based on eqn (1), whereby $Li_2TP$ reacted with oxygen to yield $Li_2CO_3$ and $CO_2$ emissions.[46] Transition metal terephthalates similarly react with oxygen, resulting in the production of metal oxides and $CO_2$ (eqn (1) and (2)).[26]

$$2LiOOCC_6H_4COOLi + 13O_2 \rightarrow 2Li_2CO_3 + 12CO_2 + H_2O^{48} \quad (1)$$

$$2TMC_6H_4(COO)_2 + 17O_2 \rightarrow 2TMO + 16CO_2 + 4H_2O^{48,59-61} \quad (2)$$

The sintering process was regulated to maintain a heating rate of 5 °C $min^{-1}$ to 600 °C. The sintered powder was dissolved in DI water at room temperature. After filtration, the lithium carbonate solution was obtained. This solution, upon transfer into acetone (the volume ratio of acetone to $Li_2CO_3$ solution was established at 1 : 1), allowed for the recrystallization of lithium carbonate. The recovered lithium carbonate powder was then washed with acetone solution during the filtration process and subsequently dried in a conventional oven. To purify the utilized acetone solution, a distillation process was employed, based on the boiling points of the involved substances.

### Materials characterization

Elemental concentrations within all leaching solutions, recycled chemicals, and end products were quantitatively assessed using Inductively Coupled Plasma Optical Emission Spectrometry (ICP-OES) to confirm efficiency and degree of purification (Horiba 2). The crystalline structures of particles were investigated through X-ray Powder Diffraction (XRD) analysis, employing a PANalytical Empyrean system with a Cu Kα radiation source ($\lambda = 1.54$ Å) and a scanning increment of 0.0167°. Scanning Electron Microscopy (SEM; JSM 7000F SEM) was utilized to evaluate the morphology and particle size. To confirm the chemical composition of the product after extraction rection, Nuclear Magnetic Resonance (NMR, 500 MHz 3-channel Bruker Avance Neo) spectroscopy was performed. Thermal behaviour and compositional changes of the dilithium terephthalate contaminants were examined using a Simultaneous Thermal Analyzer (SDT Q600-TA Instruments), which records both thermal transitions and mass variations in relation to temperature (or time) within a dry air environment. X-ray Photoelectron Spectroscopy (XPS) analyses were carried out with a PHI 500 VersaProbe II apparatus from Physical Electronics to elucidate the oxidation states of metallic elements on the particle surfaces, with spectral fittings processed *via* XPSpeak41 software. Focused ion beam (FIB) imaging and advanced scanning electron microscopy (SEM) were conducted using a Thermo Scientific Scios 2 DualBeam system for cross-section preparation and scanning images.

### Electrochemical testing

The electrode composition was formulated with active material (93 wt%), conductive carbon black ($C_{65}$) at 4 wt%, and polyvinylidene fluoride (PVDF) binder constituting the remaining 3 wt%, and all dispersed in *N*-methyl-2-pyrrolidone (NMP) solvent to create a homogeneous slurry. This slurry was then spread over aluminium foil, followed by a drying process at 80 ° C for 1 hour in a conventional oven to evaporate any solvent compound. Subsequently, the dried casting was calendared and cut into electrodes of square shapes, 57 mm by 44 mm (for single layer pouch cells), respectively. Each electrode was precisely weighed to confirm a uniform mass loading of about 18 mg $cm^{-2}$. Prior to assembly, these electrodes were further dried at 120 °C for 12 hours under vacuum condition.

The assembly for single layer pouch cells was undertaken in a glovebox. This procedure included the assembling of cathodes, complemented by a separator, electrolyte, and graphite anode. The single layer pouch cells underwent electrochemical performance assessment over a comprehensive range of discharge rates, from C/20 up to 2C. Whereas the cycling stability evaluations were operated at a consistent charging/discharging rate of 0.5C. These tests were conducted within a voltage range of 2.8 to 4.2 V under room temperature.

## Data availability

The data supporting the findings of this study were generated from experiments conducted by the authors. All relevant datasets have been included in the manuscript and ESI.† Additional raw data and analysis scripts are available upon reasonable request from the corresponding author.

## Author contributions

The contributions to this project are as follows: Jiahui Hou and Zexin Wang were involved in conceptualization, investigation, methodology, and the writing of the original draft. Zifei Meng, Jinzhao Fu, Zeyi Yao, Wenting Jin, and Xiaotu Ma contributed through investigation, and validation. Zhenzhen Yang specifically carried out the investigation of XPS analysis. Yan Wang played a crucial role in funding acquisition, provided supervision, and also reviewed and edited the manuscript.

## Conflicts of interest

There is a patent application based on the research results reported in this paper.

## Acknowledgements

The authors gratefully acknowledge the help from Materials and Device Evaluation group at Argonne National Laboratory, supported by the U.S. DOE Vehicle Technologies office, under contract number DE-AC02-06CH11357.

## References

1 X. Zheng, Z. Zhu, X. Lin, Y. Zhang, Y. He, H. Cao and Z. Sun, A mini-review on metal recycling from spent lithium ion batteries, *Engineering*, 2018, **4**(3), 361–370.
2 L. Paoli; T. Gül, *Electric Cars Fend off Supply Challenges to More than Double Global Sales*, 2022.
3 D. Latini, M. Vaccari, M. Lagnoni, M. Orefice, F. Mathieux, J. Huisman, L. Tognotti and A. Bertei, A comprehensive review and classification of unit operations with assessment of outputs quality in lithium-ion battery recycling, *J. Power Sources*, 2022, **546**, 231979.
4 M. Chen, X. Ma, B. Chen, R. Arsenault, P. Karlson, N. Simon and Y. Wang, Recycling End-of-Life Electric Vehicle Lithium-Ion Batteries, *Joule*, 2019, **3**(11), 2622–2646.
5 B. Huang, Z. Pan, X. Su and L. An, Recycling of lithium-ion batteries: Recent advances and perspectives, *J. Power Sources*, 2018, **399**, 274–286.
6 B. Scrosati and J. Garche, Lithium batteries: Status, prospects and future, *J. Power Sources*, 2010, **195**(9), 2419–2430.
7 M. Wentker, M. Greenwood and J. Leker, A bottom-up approach to lithium-ion battery cost modeling with a focus on cathode active materials, *Energies*, 2019, **12**(3), 504.
8 Survey, U. S. G., *Mineral Commodity Summaries*, 2024.
9 E. Fan, L. Li, J. Lin, J. Wu, J. Yang, F. Wu and R. Chen, Low-temperature molten-salt-assisted recovery of valuable metals from spent lithium-ion batteries, *ACS Sustainable Chem. Eng.*, 2019, **7**(19), 16144–16150.
10 J. F. Paulino, N. G. Busnardo and J. C. Afonso, Recovery of valuable elements from spent Li-batteries, *J. Hazard. Mater.*, 2008, **150**(3), 843–849.
11 W. Lv, Z. Wang, H. Cao, Y. Sun, Y. Zhang and Z. Sun, A critical review and analysis on the recycling of spent lithium-ion batteries, *ACS Sustain. Chem. Eng.*, 2018, **6**(2), 1504–1521.
12 J. Xiao, J. Li and Z. Xu, Challenges to future development of spent lithium ion batteries recovery from environmental and technological perspectives, *Environ. Sci. Technol.*, 2019, **54**(1), 9–25.
13 X. Zhang, Y. Bian, S. Xu, E. Fan, Q. Xue, Y. Guan, F. Wu, L. Li and R. Chen, Innovative application of acid leaching to regenerate Li (Ni1/3Co1/3Mn1/3) O2 cathodes from spent lithium-ion batteries, *ACS Sustain. Chem. Eng.*, 2018, **6**(5), 5959–5968.
14 Q. Cheng, Z. Wang, Y. Wang, J.-T. Li and H. Fu, Recent advances in preferentially selective Li recovery from spent lithium-ion batteries: A review, *J. Environ. Chem. Eng.*, 2024, **12**(3), 112903.
15 L. Chen, Y. Chao, X. Li, G. Zhou, Q. Lu, M. Hua, H. Li, X. Ni, P. Wu and W. Zhu, Engineering a tandem leaching system for the highly selective recycling of valuable metals from spent Li-ion batteries, *Green Chem.*, 2021, **23**(5), 2177–2184.
16 Q. Jing, J. Zhang, Y. Liu, C. Yang, B. Ma, Y. Chen and C. Wang, E-pH Diagrams for the Li-Fe-P-H2O System from 298 to 473 K: Thermodynamic Analysis and Application to the Wet Chemical Processes of the LiFePO4 Cathode Material, *J. Phys. Chem. C*, 2019, **123**(23), 14207–14215.
17 X. Qiu, B. Zhang, Y. Xu, J. Hu, W. Deng, G. Zou, H. Hou, Y. Yang, W. Sun and Y. Hu, Enabling the sustainable recycling of LiFePO 4 from spent lithium-ion batteries, *Green Chem.*, 2022, **24**(6), 2506–2515.
18 I. Perdana, D. R. Aprilianto, F. A. Fadillah, R. Fadli, H. T. B. M. Petrus, W. Astuti, M. A. Muflikhun, H. Nilasary, H. S. Oktaviano, F. Fathoni, E. Raihan and S. U. Muzayanha, Lithium recovery from mixed spent LFP-NMC batteries through atmospheric water leaching, *Sci. Rep.*, 2025, **15**(1), 2591.
19 L. Li, J. Ge, F. Wu, R. Chen, S. Chen and B. Wu, Recovery of cobalt and lithium from spent lithium ion batteries using organic citric acid as leachant, *J. Hazard. Mater.*, 2010, **176**(1), 288–293.
20 L. Li, J. Ge, F. Wu, R. Chen, S. Chen and B. Wu, Recovery of cobalt and lithium from spent lithium ion batteries using organic citric acid as leachant, *J. Hazard. Mater.*, 2010, **176**(1–3), 288–293.
21 M. Yu, Z. Zhang, F. Xue, B. Yang, G. Guo and J. Qiu, A more simple and efficient process for recovery of cobalt and lithium from spent lithium-ion batteries with citric acid, *Sep. Purif. Technol.*, 2019, **215**, 398–402.
22 X. Chen and T. Zhou, Hydrometallurgical process for the recovery of metal values from spent lithium-ion batteries in citric acid media, *Waste Manage. Res.*, 2014, **32**(11), 1083–1093.
23 T. Punt, G. Akdogan, S. Bradshaw and P. van Wyk, Development of a novel solvent extraction process using citric acid for lithium-ion battery recycling, *Miner. Eng.*, 2021, **173**, 107204.
24 L. M. J. Rouquette, M. Petranikova and N. Vieceli, Complete and selective recovery of lithium from EV lithium-ion batteries: Modeling and optimization using oxalic acid as a leaching agent, *Sep. Purif. Technol.*, 2023, **320**, 124143.
25 J. Hou, X. Ma, J. Fu, P. Vanaphuti, Z. Yao, Y. Liu, Z. Yang and Y. Wang, A green closed-loop process for selective recycling of lithium from spent lithium-ion batteries, *Green Chem.*, 2022, **24**(18), 7049–7060.
26 F. G. Sherif, Heavy metal terephthalates, *Ind. Eng. Chem. Prod. Res. Dev.*, 1970, **9**(3), 408–412.
27 G. L. Ball, C. J. McLellan and V. S. Bhat, Toxicological review and oral risk assessment of terephthalic acid (TPA) and its esters: A category approach, *Crit. Rev. Toxicol.*, 2012, **42**(1), 28–67.
28 J. Pang, M. Zheng, R. Sun, A. Wang, X. Wang and T. Zhang, Synthesis of ethylene glycol and terephthalic acid from biomass for producing PET, *Green Chem.*, 2016, **18**(2), 342–359.

 

29 M. J. Kaiser; E. W. McAllister, 6 - Pigging, Cleaning & Drying, in *Pipeline Rules of Thumb Handbook*, ed. M. J. Kaiser, E. W. McAllister, Gulf Professional Publishing, 9th edn, 2023, pp 217–246.

30 M. Boscoianu, G. Prelipcean and M. Lupan, Innovation enterprise as a vehicle for sustainable development – A general framework for the design of typical strategies based on enterprise systems engineering, dynamic capabilities, and option thinking, *J. Cleaner Prod.*, 2018, **172**, 3498–3507.

31 Y. Su, Q. Zheng, Y. Suga and M. Watanabe, Measurement of solubility of terephthalic acid in water under hydrothermal conditions, *J. Supercrit. Fluids*, 2025, **218**, 106497.

32 E. I. M. Bardoquillo, J. M. B. Firman, D. B. Montecastro and A. M. Basilio, Chemical recycling of waste polyethylene terephthalate (PET) bottles via recovery and polymerization of terephthalic acid (TPA) and ethylene glycol (EG), *Mater. Today: Proc.*, 2023, DOI: **10.1016/j.matpr.2023.04.160**.

33 Z. Chen, J. Wang, D. Chao, T. Baikie, L. Bai, S. Chen, Y. Zhao, T. C. Sum, J. Lin and Z. Shen, Hierarchical Porous LiNi1/3Co1/3Mn1/3O2 Nano-/Micro Spherical Cathode Material: Minimized Cation Mixing and Improved Li+ Mobility for Enhanced Electrochemical Performance, *Sci. Rep.*, 2016, **6**(1), 25771.

34 X. Wang, H. Zhou, Z. Chen and X. Meng, Synchrotron-based X-ray diffraction and absorption spectroscopy studies on layered LiNixMnyCozO2 cathode materials: A review, *Energy Storage Mater.*, 2022, **49**, 181–208.

35 W.-S. Yoon, K. Y. Chung, J. McBreen and X.-Q. Yang, A comparative study on structural changes of LiCo1/3Ni1/3Mn1/3O2 and LiNi0. 8Co0. 15Al0. 05O2 during first charge using in situ XRD, *Electrochem. Commun.*, 2006, **8**(8), 1257–1262.

36 K.-W. Nam, W.-S. Yoon, H. Shin, K. Y. Chung, S. Choi and X.-Q. Yang, In situ X-ray diffraction studies of mixed LiMn2O4–LiNi1/3Co1/3Mn1/3O2 composite cathode in Li-ion cells during charge–discharge cycling, *J. Power Sources*, 2009, **192**(2), 652–659.

37 P.-Y. Liao, J.-G. Duh, J.-F. Lee and H.-S. Sheu, Structural investigation of Li1− xNi0. 5Co0. 25Mn0. 25O2 by in situ XAS and XRD measurements, *Electrochim. Acta*, 2007, **53**(4), 1850–1857.

38 B. Jeevanantham, P. Sarathkumar, S. Kavita and M. K. Shobana, Magnesium doped LiNixMnyCozO2 cathode- structural properties, *Appl. Surf. Sci. Adv.*, 2022, **12**, 100350.

39 W. M. Dose, I. Temprano, J. P. Allen, E. Björklund, C. A. O'Keefe, W. Li, B. L. Mehdi, R. S. Weatherup, M. F. L. De Volder and C. P. Grey, Electrolyte Reactivity at the Charged Ni-Rich Cathode Interface and Degradation in Li-Ion Batteries, *ACS Appl. Mater. Interfaces*, 2022, **14**(11), 13206–13222.

40 I. de Meatza, I. Landa-Medrano, S. Sananes-Israel, A. Eguia-Barrio, O. Bondarchuk, S. Lijó-Pando, I. Boyano, V. Palomares, T. Rojo, H.-J. Grande and I. Urdampilleta, *Influence of the Ambient Storage of LiNi0.8Mn0.1Co0.1O2 Powder and Electrodes on the Electrochemical Performance in Li-Ion Technology Batteries*, 2022.

41 P. Xu, X. Guo, B. Jiao, J. Chen, M. Zhang, H. Liu, X. Yu, M. Appleberry, Z. Yang, H. Gao, F. Yang, X. Weng, Y. Shen, J. Gu, Y. S. Meng, C. Brooks, S. P. Ong and Z. Chen, Proton-exchange induced reactivity in layered oxides for lithium-ion batteries, *Nat. Commun.*, 2024, **15**(1), 9842.

42 B. Xu, D. Qian, Z. Wang and Y. S. Meng, Recent progress in cathode materials research for advanced lithium ion batteries, *Mater. Sci. Eng., R*, 2012, **73**(5–6), 51–65.

43 L. Qiao, U. Oteo, M. Martinez-Ibañez, A. Santiago, R. Cid, E. Sanchez-Diez, E. Lobato, L. Meabe, M. Armand and H. Zhang, Stable non-corrosive sulfonimide salt for 4-V-class lithium metal batteries, *Nat. Mater.*, 2022, **21**(4), 455–462.

44 D. Ko and S. Mhin, Effect of One Step Solid State Reaction Route on the Semiconductor Behavior of the Spinel (NI, Co, and Mn)O4 to Be Used as Temperature Sensor, *Sensors*, 2023, **23**, 5380.

45 H. H. Lee, Y. Park, S. H. Kim, S.-H. Yeon, S. K. Kwak, K. T. Lee and S. Y. Hong, Mechanistic Studies of Transition Metal-Terephthalate Coordination Complexes upon Electrochemical Lithiation and Delithiation, *Adv. Funct. Mater.*, 2015, **25**(30), 4859–4866.

46 L. Kumaresan, K. Kasiviswanathan, K. P. Kirubakaran, M. Priyadarshini, K. Mathiyalagan, C. Senthil, C. W. Lee and K. Vediappan, Band-Gap Tuned Dilithium Terephthalate from Environmentally Hazardous Material for Sustainable Lithium Storage Systems with DFT Modelling, *ChemistrySelect*, 2022, **7**(25), e202200527.

47 S. Zhang, S. Ren, D. Han, M. Xiao, S. Wang and Y. Meng, Aqueous sodium alginate as binder: Dramatically improving the performance of dilithium terephthalate-based organic lithium ion batteries, *J. Power Sources*, 2019, **438**, 227007.

48 G. P. Panasyuk, L. A. Azarova, M. Khaddaj, G. P. Budova, I. L. Voroshilov, T. V. Grusha and A. D. Izotov, Preparation and Properties of Sodium, Potassium, Magnesium, Calcium, and Aluminum Terephthalates, *Inorg. Mater.*, 2003, **39**(12), 1292–1297.

49 G. Li, B. Klein, C. Sun and J. Kou, Lab-scale error analysis on X-ray fluorecence sensing for bulk ore sorting, *Miner. Eng.*, 2021, **164**, 106812.

50 A. Fahimi, S. Ducoli, S. Federici, G. Ye, E. Mousa, P. Frontera and E. Bontempi, Evaluation of the sustainability of technologies to recycle spent lithium-ion batteries, based on embodied energy and carbon footprint, *J. Cleaner Prod.*, 2022, **338**, 130493.

51 K. Matuszek, E. Pankalla, A. Grymel, P. Latos and A. Chrobok, Studies on the Solubility of Terephthalic Acid in Ionic Liquids, *Molecules*, 2020, **25**(1), 80.

52 W. Perez, H. A. C. Barrientos, C. Suarez and M. Bravo, *Method for the Production of Battery Grade Lithium Carbonate from Natural and Industrial Brines*, Google Patent, 2014.

53 X. Ma, M. Chen, Z. Zheng, D. Bullen, J. Wang, C. Harrison, E. Gratz, Y. Lin, Z. Yang, Y. Zhang, F. Wang, D. Robertson, S.-B. Son, I. Bloom, J. Wen, M. Ge, X. Xiao, W.-K. Lee,

M. Tang, Q. Wang, J. Fu, Y. Zhang, B. C. Sousa, R. Arsenault, P. Karlson, N. Simon and Y. Wang, Recycled cathode materials enabled superior performance for lithium-ion batteries, *Joule*, 2021, **5**(11), 2955–2970.

54 *Purified Terephthatic Acid (PTA) Market Analysis: Insudtru Market Size, Plant Capacity, Production, Operating Efficiency, Demand & Supply, End-User Industries, Sales Channel, Regional Demand*, Foreign Trade, Comparny Share, Manufacturing Process, 2023, pp. , pp. 2015–2032.

55 D. Celante, L. O. Diehl, L. N. Brondani, C. A. Bizzi and F. de Castilhos, Measurement and Correlation of the Solubility of Terephthalic Acid in Six Pure Solvents and Five Binary Mixtures, *J. Chem. Eng. Data*, 2021, **66**(9), 3512–3519.

56 Q.-b. Wang, H.-b. Xu and X. Li, Solubility of terephthalic acid in aqueous acetic acid from 423.15 to 513.15 K, *Fluid Phase Equilib.*, 2005, **233**(1), 81–85.

57 T. H. Nguyen and M. S. Lee, A Review on the Separation of Lithium Ion from Leach Liquors of Primary and Secondary Resources by Solvent Extraction with Commercial Extractants, *Processes*, 2018, **6**(5), 55.

58 L. Wang, C. Mou, B. Wu, J. Xue and J. Li, Alkaline Earth Metal Terephthalates MC8H4O4 (M=Ca, Sr, Ba) as Anodes for Lithium Ion Batteries, *Electrochim. Acta*, 2016, **196**, 118–124.

59 G. A. M. Hussein, A. K. H. Nohman and K. M. A. Attyia, Characterization of the decomposition course of nickel acetate tetrahydrate in air, *J. Therm. Anal.*, 1994, **42**(6), 1155–1165.

60 G. A. El-Shobaky, K. A. El-Barawy and A. A. Ibrahim, Thermal solid—solid interaction between sodium and manganese oxides, *Thermochim. Acta*, 1986, **101**, 195–203.

61 Z. Ouyang, P. Wen, Y. Chen and L. Ye, Study on thermodynamic equilibrium and character inheritance of cobalt carbonate decomposition, *Vacuum*, 2020, **179**, 109559.

 